Unidirectional dielectric resonator antenna using 3-D-printed uniaxial anisotropic ceramic

Carlos David Morales Peña, Audric Boiteau, Christophe Morlaas, Alexandre Chabory, Romain Pascaud, Marjorie Grzeskowiak, Gautier Mazingue

IET Microwaves, Antennas & Propagation

WILEY

The Institution of Engineering and Technology

ORIGINAL RESEARCH OPEN ACCESS

Unidirectional Dielectric Resonator Antenna Using 3-D-Printed Uniaxial Anisotropic Ceramic

Carlos David Morales Peña[1,2] | Audric Boiteau[1,2] | Christophe Morlaas[1] | Alexandre Chabory[1] | Romain Pascaud[2] | Marjorie Grzeskowiak[2] | Gautier Mazingue[3]

[1]ENAC, Université de Toulouse, Toulouse, France | [2]ISAE-SUPAERO, Université de Toulouse, Toulouse, France | [3]ANYWAVES, Toulouse, France

Correspondence: Romain Pascaud (romain.pascaud@isae-supaero.fr)

Received: 14 November 2024 | **Revised:** 21 March 2025 | **Accepted:** 7 April 2025

Handling Editor: Neng-Wu Liu

Funding: This research received grants from the 'Ecole Nationale de l'Aviation Civile' and the 'Région Occitanie Pyrénées-Méditerranée'.

Keywords: anisotropic media | dielectric resonator antennas | three-dimensional printing

ABSTRACT

A Huygens source dielectric resonator antenna (DRA) with unidirectional radiation pattern is presented. It consists of a coaxial probe exciting a rectangular, homogeneous and uniaxial anisotropic dielectric resonator (DR). To obtain a Huygens source radiation pattern, a pair of quasi-TM and TE modes are combined by controlling the permittivity tensor of the DR. A prototype operating at 2.5 GHz has been designed. The DR is made up of periodic anisotropic unit cells on a subwavelength scale and fabricated using a three-dimensional (3-D) printer. The simulated and measured results are in reasonable agreement. A relative impedance bandwidth of 12.5% and a front-to-back ratio larger than 15 dB at operating frequency are finally measured.

1 | Introduction

New small aerial or space platforms, such as unmanned aerial vehicles (UAVs) or CubeSats, have few or no metallic surfaces that can act as the ground plane for the integrated antennas, a factor that generally affects their performance [1, 2]. Complementary dipole antennas eliminate the need for a ground plane while obtaining interesting antenna properties, such as quasi-isotropic radiation [3, 4], polarisation diversity [5] or controlled beam scanning [6, 7]. Among these solutions, Huygens source antennas provide a unidirectional cardioid-shaped radiation pattern with a large front-to-back (F/B) ratio and an omnidirectional polarisation purity [8, 9]. To do so, they combine co-located elementary electric and magnetic dipoles of the same radiation intensity but with an orthogonal orientation and a specific phase shift between them. For a linearly polarised (LP) Huygens source, only one electric and one magnetic dipoles are required [10–12], whereas to achieve circular polarisation, at least two electric and two magnetic dipoles are needed [9, 13, 14].

Recently, several Huygens source dielectric resonator antennas (DRA) have been proposed due to their attractive features such as small size, low loss and relatively wide bandwidth [15–19]. The elementary electric dipole is generally due to the radiation from the coaxial probe, whereas the magnetic dipole relies on the excitation of a specific resonant mode in the dielectric resonator (DR). As a result, these solutions exhibit unilateral radiation with the main lobe perpendicular to the coaxial probe, that is, to say lateral radiation, and they do not allow radiation in the broadside direction.

To overcome this limitation, it is necessary to excite an elementary electric dipole perpendicular to the coaxial feeding probe. One solution is to use parasitic metallic ground or elements in addition to the DR [20–22]. However, these antennas

can be sensitive to coupling between resonant metal elements and nearby objects. Recently, the authors have proposed a solution for having unilateral radiation in the broadside direction [23]. This solution stacks two isotropic DRs with different sizes and permittivities to obtain in each of them the specific resonant modes that are equivalent to the required elementary dipoles. Nevertheless, this DRA has nonco-located elementary dipoles and still suffers from a lack of symmetry in its radiation pattern.

Concurrently, the 3-D printing of dielectric materials has been explored in the literature, bringing new perspectives in the control of their properties such as permittivity value [24, 25], inhomogeneity [26, 27], anisotropy [28, 29] or dispersion [30]. When applied to DRAs, it provides greater design flexibility to achieve wideband [31, 32], multiband [33], circular polarisation [34, 35] or array configurations [36–38]. In particular, uniaxial anisotropic DRAs have already been proposed to increase the antenna gain [39–44] or half-power beamwidth [45] or to achieve circular polarisation at one [46] or two frequency bands [47]. However, note that only the two last DRs have been 3-D-printed.

In this paper, we propose a Huygens source DRA using a 3-D-printed uniaxial anisotropic DR. In our case, the anisotropy is used to control almost independently the resonance frequencies of several resonant modes of the DR [48]. More specifically, two selected modes are responsible for generating a broadside cardioid-shaped radiation pattern in z-direction by providing elementary equivalent electric and magnetic dipoles radiation. Consequently, this Huygens source DRA relies solely on the use of co-located DR modes and not on additional ground or feed radiation, and it achieves a 16% reduction in size compared to the solution presented in ref. [23]. A prototype has been designed at 2.5 GHz and 3-D-printed. Its reflection coefficient, radiation patterns and antenna gain have been simulated and measured with a good agreement.

The paper is organised as follows. Section 2 describes the working principle of the proposed Huygens source DRA. Specifically, in Section 3, uniaxial anisotropic DRs are addressed to study the effects of an additional degree of freedom. From this analysis, an antenna design is proposed in Section 4 and its practical implementation through 3-D printing is discussed. Then, measurements and simulation results are compared in Section 5. Finally, conclusions are presented in Section 6.

2 | Huygens Source Principle

To obtain a linearly polarised Huygens source pattern, we need to combine two co-located and orthogonal elementary electric and magnetic dipoles. For a unidirectional cardioid-shaped radiation pattern, an amplitude balance and a phase shift of 0° or 180° are required between the two elementary dipoles, depending on the main direction of radiation.

For instance, the radiated far field in spherical coordinate for an elementary electric dipole along the y-direction is

$$\boldsymbol{E_{ey}} = p_e \eta_0 A\left(\cos\theta \sin\phi\hat{\boldsymbol{\theta}} + \cos\phi\hat{\boldsymbol{\phi}}\right) \tag{1}$$

with p_e its electric dipole moment, η_0 the impedance of free space and $A = \frac{k_0^2 c_0}{4\pi r} e^{-\mathrm{j}k_0 r}$. The radiated far field from an elementary magnetic dipole along the x-direction is

$$\boldsymbol{E_{mx}} = p_m A\left(\sin\phi\hat{\boldsymbol{\theta}} + \cos\theta\cos\phi\hat{\boldsymbol{\phi}}\right) \tag{2}$$

with p_m its magnetic dipole moment.

Assuming $p_m = \eta_0 e^{\mathrm{j}\delta} p_e$ with a phase difference $\delta = 180°$ between both dipole moments, we obtain the magnitude of the total radiated far field

$$|\boldsymbol{E}_{\mathrm{tot}}| = |p_m||A|(1 + \cos\theta). \tag{3}$$

Equation (3) represents a cardioid-shaped LP radiation pattern with its main radiation in $\theta = 0°$ and a maximal theoretical directivity of 4.77 dBi [49].

It is here intended to use two resonant modes of a single DR to obtain these co-located elementary dipoles without depending on ground or feed radiation. Assuming a rectangular DR, the two equivalent elementary magnetic and electric dipoles can be excited using the $\mathrm{TE}^x_{\delta 11}$ mode and a higher order mode that will be named quasi-TM^y, respectively. More specifically, the quasi-TM^y mode results from the $\mathrm{TE}^x_{\delta 12}$ and $\mathrm{TE}^z_{21\delta}$ modes by imposing a square cross-section transverse to the y-direction, whose combination spawns the former mode alongside with a quasi-HEM mode [50]. It is important to note that it is not mandatory to feed the DR with a central probe to excite the quasi-TM^y mode but that it is sufficient to locate the excitation current where the modal electric field is neither orthogonal nor zero [51, 52].

3 | Uniaxial Anisotropic Dielectric Resonator

To fulfil the Huygens source conditions using quasi-TM^y and $\mathrm{TE}^x_{\delta 11}$ modes in a single DR, a new degree of freedom is provided by considering a homogeneous uniaxial anisotropic DR with the relative permittivity tensor

$$\overline{\overline{\varepsilon_r}} = \begin{bmatrix} \varepsilon_{ro} & 0 & 0 \\ 0 & \varepsilon_{ry} & 0 \\ 0 & 0 & \varepsilon_{ro} \end{bmatrix}. \tag{4}$$

The y-axis is chosen here as the extraordinary axis (uniaxial-y medium) to retain the geometrical degeneracy of the $\mathrm{TE}^x_{\delta 12}$ and $\mathrm{TE}^z_{21\delta}$ modes from which the quasi-TM^y stems. It is important to note that in a uniaxial-y medium, it is theoretically not possible to define pure TE^x and TE^z modes for a rectangular DR. However, since the existing hybrid modes field distributions remain similar in the simulation results, we will refer to them as TE modes in the following for simplicity.

First, for a given relative permittivity $\varepsilon_r = 13$, we can determine the dimensions $a \times b \times a$ of an isotropic DR represented on Figure 1a so that its $\mathrm{TE}^x_{\delta 11}$ mode resonates at a frequency close to the operating frequency of the desired antenna, for instance, $f_{0,\mathrm{TE}^x_{\delta 11}} = 2.5$ GHz. The ordinary relative permittivity is then kept at $\varepsilon_{rx} = \varepsilon_{rz} = \varepsilon_{ro} = 13$, and three values of DR height a are

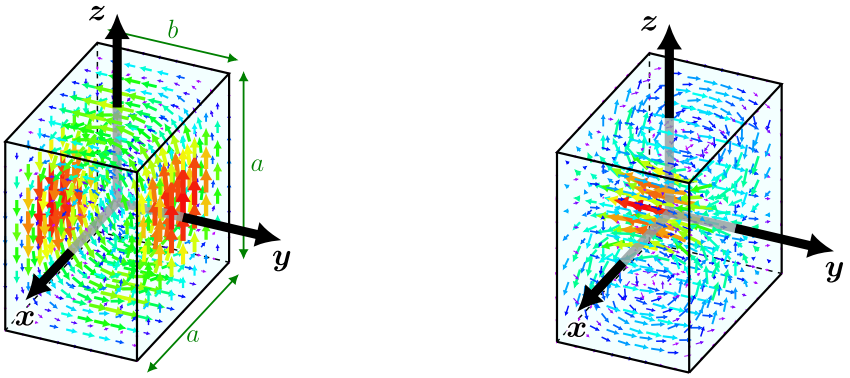

(a) $\mathrm{TE}^{x}_{\delta 11}$ mode (b) quasi-TM^{y} mode

FIGURE 1 | Schematic representation of the electric field distribution of the (a) $\mathrm{TE}^{x}_{\delta 11}$ and (b) quasi-TM^{y} modes in a rectangular DR.

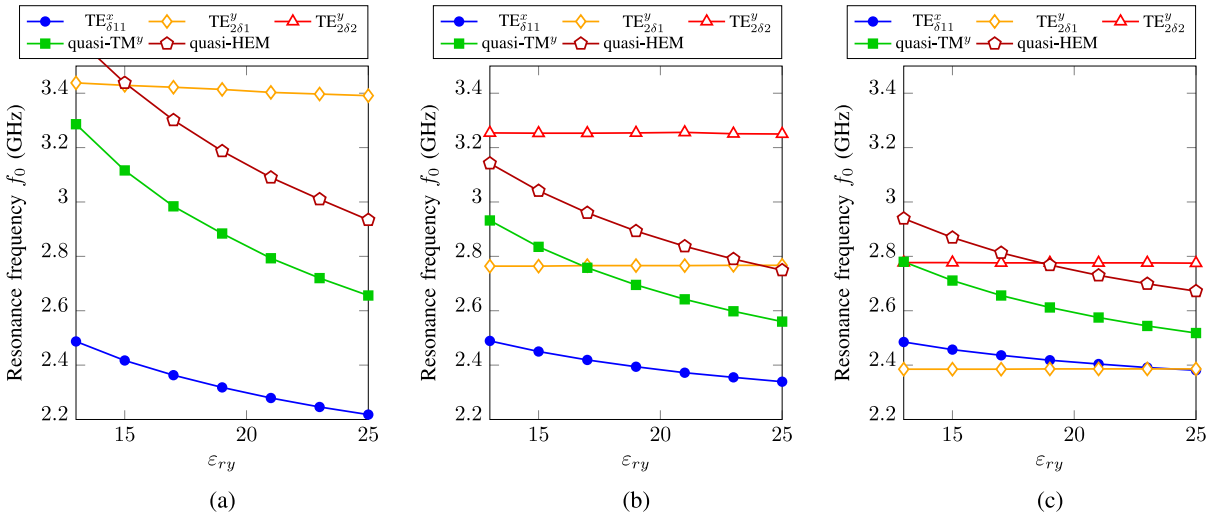

FIGURE 2 | Simulated resonance frequencies of the modes of interest ($\mathrm{TE}^{x}_{\delta 11}$ and quasi-TM^{y}) and others in vicinity ($\mathrm{TE}^{y}_{2\delta 1}$, quasi-HEM and $\mathrm{TE}^{y}_{2\delta 2}$) as a function of ε_{ry}, for different values of the aspect ratio $\frac{a}{b}$, resulting from an Eigenmode analysis and considering $\varepsilon_{ro} = 13$. Missing modes are out of scope in higher frequencies. (a) $\frac{a}{b} = 1.2$, with $a = 29.0$ mm. (b) $\frac{a}{b} = 2.1$, with $a = 39.6$ mm. (c) $\frac{a}{b} = 2.8$, with $a = 49.0$ mm.

chosen to analyse the effects of the aspect ratio a/b. Figure 2 shows that increasing ε_{ry} leads to a greater decrease in the resonance frequency of the quasi-TM^{y} mode than for the $\mathrm{TE}^{x}_{\delta 11}$ mode, enabling the frequency shift between the two modes to be tuned. This can be explained by noticing in Figure 1b that the dominant E-field component of the quasi-TM^{y} mode is collinear to the y-axis, making it particularly sensitive to the extraordinary relative permittivity ε_{ry}. One can note that a smaller frequency difference can be more easily obtained with a higher aspect ratio as shown in Figure 2c. The main downsides are an increase of the DR height, hindering profile reduction goals, but also the convergence of higher order modes towards the operating frequency that may bring spurious effects. Conversely, a smaller aspect ratio is analysed in Figure 2a and displays the difficulty to bring required modes closer without using an important value of birefringence.

4 | Huygens Source Antenna

The DR anisotropy has been used to control almost independently the resonance frequencies of the quasi-TM^{y} and $\mathrm{TE}^{x}_{\delta 11}$ modes, which are expected to provide elementary equivalent electric and magnetic dipoles, respectively, for Huygens source radiation. In this section, the design of the Huygens source DRA is presented, including its feeding, as well as its implementation through 3-D printing.

4.1 | Design

Figure 3 shows the proposed Huygens source DRA. It consists of a single uniaxial anisotropic DR, a thin dielectric layer (Rogers RO3003 with $\varepsilon_r = 3.0$ and $\tan\delta = 0.001$) and a semi-rigid coaxial probe (RG405). The final dimensions of the DR are $a = 39.6$ mm and $b = 19.2$ mm, namely $\frac{a}{b} \approx 2.1$ and an electrical size of $0.33\lambda_0$ and $0.16\lambda_0$ at $f_0 = 2.5$ GHz.

One can note that in order to have both equivalent dipoles match the Huygens source conditions, the difference in resonance frequencies of the required modes shall not be nullified but reduced to a particular value. Eventually, an optimum can be found to satisfy user-defined goals on both radiation

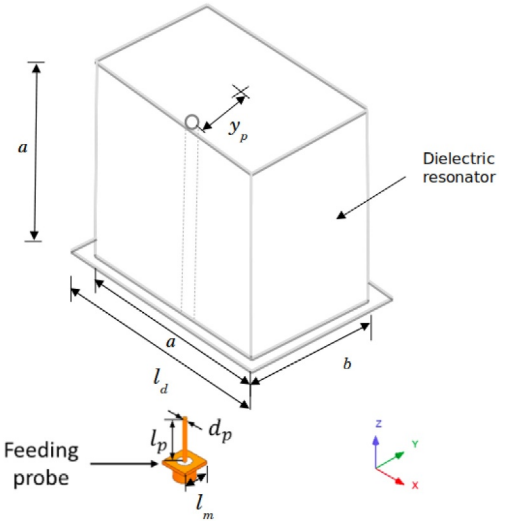

FIGURE 3 | Schematic of the Huygens source DRA ($a = 39.6$, $b = 19.2$, $l_d = 43.4$, $l_p = 17.6$, $d_p = 0.51$, $l_m = 6$ and $y_p = 8.5$ mm).

properties and dimensions. As shown in Figure 4, the maximum F/B ratio at 2.5 GHz is obtained using a uniaxial anisotropic dielectric having a permittivity tensor with $\varepsilon_{ry} \approx 21$ and $\varepsilon_{ro} = 13$ alongside with previously stated dimensions. The Eigenmode analysis of the described DR is related to the intermediate case depicted in Figure 2b; hence, the Huygens source operating frequency f_0 appears to be close to the centre of the 270-MHz frequency difference between the resonance frequencies of the $TE^x_{\delta 11}$ and quasi-TM^y modes.

The 0.75-mm thick dielectric plate supporting a small $l_m = 6$ mm square metal plate printed at its bottom is used here for mechanical purposes, notably to solder the coaxial outer conductor on one side and to glue the DR on the other.

The 50 Ω coaxial probe is located on the edge of the resonator, at a distance $y_p = 8.5$ mm, to excite both the $TE^x_{\delta 11}$ and quasi-TM^y modes. Its inner conductor has a length l_p of 17.6 mm. The location and length of the probe have been determined by a numerical parametric study.

4.2 | Implementation

The uniaxial anisotropic permittivity tensor has so far been directly assigned on Ansys HFSS. However, these values are not necessarily available with natural materials. To solve this problem, it is proposed to use 3-D-printed periodic sub-wavelength unit cells, mixing zirconia ($\varepsilon_r = 32.5$ and $\tan\delta = 0.00019$ at 10 GHz) and air to create this artificial anisotropic dielectric [46, 53].

Figure 5 shows the anisotropic cubic unit cell. Its side a_{uc}, which also corresponds to the periodicity of the artificial dielectric, is equal to 3.5 mm. For its analysis, periodic boundary conditions and Floquet ports are used on Ansys HFSS, and the effective relative permittivity tensor $\overline{\overline{\varepsilon}}_{r,\text{eff}}$ is retrieved using simulated S-parameters and a homogenisation method [54]. This approach remains accurate as long as the unit cell is electrically small,

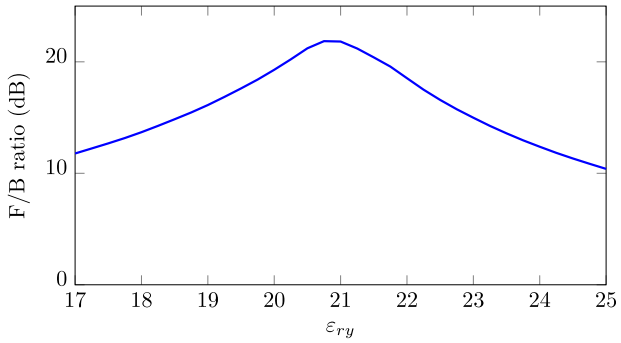

FIGURE 4 | Simulated F/B ratio of the Huygens source DRA at 2.5 GHz as a function of ε_{ry} and considering $\varepsilon_{ro} = 13$.

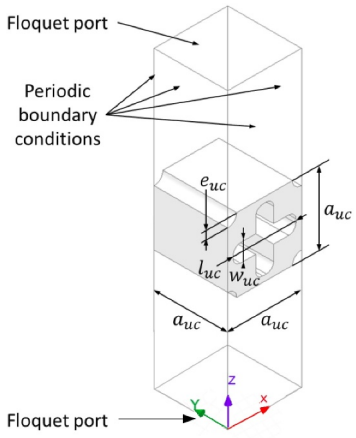

FIGURE 5 | 3-D-printed uniaxial anisotropic unit cell.

namely a side lower than $\lambda/8$, which is the case here [55, 56]. The final dimensions after optimisation are $a_{uc} = 3.5$ mm, $l_{uc} = 2.80$ mm, $w_{uc} = 0.86$ mm and $e_{uc} = 0.35$ mm.

The antenna was finally 3-D-printed using the 3-D printer C900 FLEX from 3DCERAM, which uses a stereolithography apparatus (SLA) with a photosensitive paste containing zirconia powder [57]. This 3-D printer, with a resolution of 35 μm, has already been successfully used to print anisotropic DRAs operating in the S-band [46, 47]. Figure 6 shows a picture of the 3-D-printed Huygens source DRA, namely the uniaxial anisotropic DR mounted on the small dielectric plate and fed by the coaxial probe with a quarter-wavelength sleeve to suppress stray radiation from the cable.

5 | Results

The simulated and measured reflection coefficients are shown in Figure 7. We observe good impedance matching with a measured $|S_{11}| = -18$ dB at the expected operating frequency $f_0 = 2.5$ GHz. The relative impedance bandwidth (IBW) measured with $|S_{11}| \leq -10$ dB is 12.5%. The wider impedance bandwidth in measurements is likely due to manufacturing tolerances. Notches on the $|S_{11}|$ curve around 2.8 and 2.9 GHz exist due to the contribution of excitable higher order modes tracked on Figure 2b.

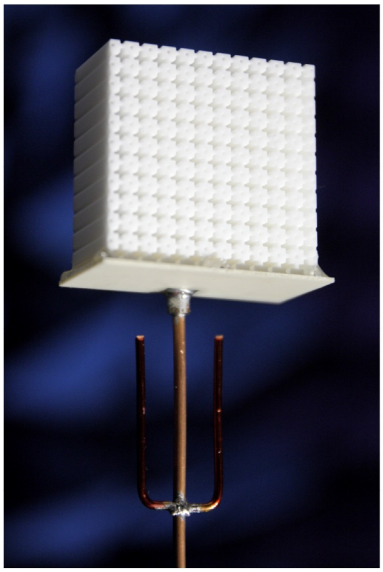

FIGURE 6 | Picture of the 3-D-printed Huygens source DRA.

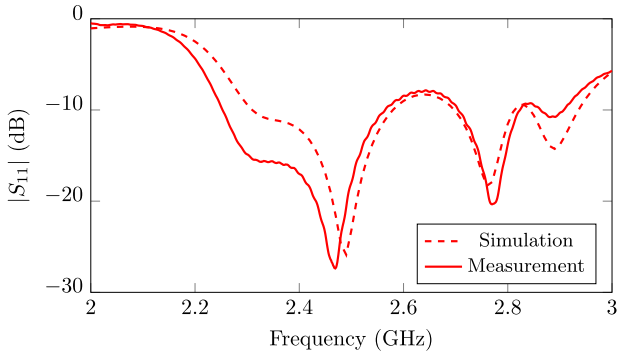

FIGURE 7 | Simulated and measured $|S_{11}|$ as a function of frequency.

Radiation patterns in $\phi = 0°$ and $\phi = 90°$ planes at 2.5 GHz are shown in Figure 8. A cardioid-shaped pattern is obtained in both planes with LP radiation. An almost perfect symmetry of the patterns is observed in the main direction of radiation, as expected for a Huygens source antenna. Some disturbances on the measured back radiation may be attributed to the dielectric mast used during measurement to hold the antenna. The high level of cross-polarisation in the $\phi = 0°$ plane may be due to stray radiation from the coaxial probe and some residual radiation of the $TE^{y}_{2\delta1}$ mode which resonates close to 2.8 GHz as shown in Figure 2b. Note that this parasitic radiation can be reduced using a differential feed, that is, to say a second coaxial probe placed symmetrically with respect to the first and fed in phase opposition [58, 59].

Figure 9 shows the antenna gain in the broadside direction as a function of frequency as well as the measured total antenna efficiency η_{tot}. The simulated and measured gains are 4.9 and 5.1 dBi, respectively, whereas the measured total efficiency is equal to 80% at 2.5 GHz.

The simulated and measured F/B ratios at 2.5 GHz are equal to 22 and 16 dB, respectively. Assuming that the F/B ratio is

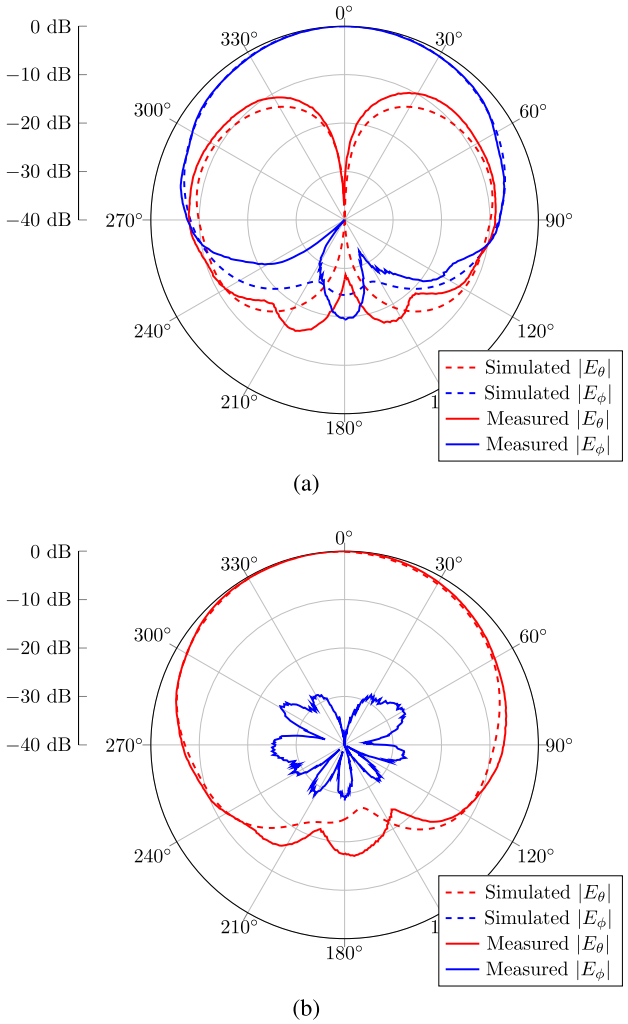

FIGURE 8 | Simulated and measured normalised radiation patterns in (a) $\phi = 0°$ and (b) $\phi = 90°$ planes at 2.5 GHz.

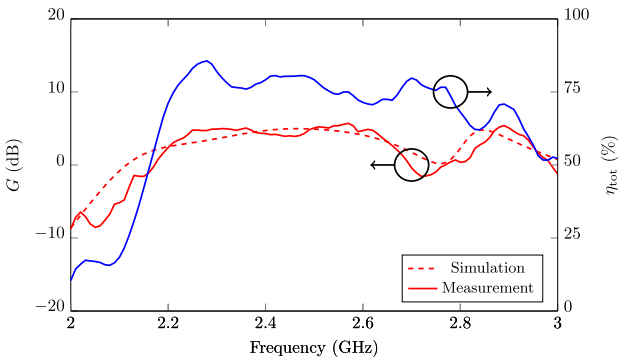

FIGURE 9 | Simulated and measured antenna gains for $\theta = \phi = 0°$ and measured total antenna efficiency as a function of frequency.

acceptable when it is greater than 15 dB, the simulated relative bandwidth of the F/B ratio is 3.2%. The measured one cannot be quantified without excessive uncertainties, since the dielectric mast supporting the antenna during measurement alters significantly the backward radiation level. Notwithstanding, we still have reasonable agreement between simulation and measurement.

TABLE 1 | Overview of unidirectional LP DRAs.

	Frequency (GHz)	ε_r	Size (λ_0^3)	Gain (dBi)	IBW	Radiation direction	Ground	p_e	p_m
[15]	2.475	15	0.38 × 0.31 × 0.23	3.9	12.1%	Lateral	Yes	Feed	DR
	3.5	15	0.56 × 0.23 × 0.43	3.4	43.6%	Lateral	Yes	Feed	DR
[20]	2.41	10	0.4 × 0.4 × 0.15	5.0	14.5%	Broadside	Yes	Ground	DR
[16]	3.55	10	0.34 × 0.34 × 0.23	4.6	28.5%	Lateral	No	Feed	DR
[18]	2.44	10	0.35 × 0.20 × 0.19	2.1	13.2%	Lateral	Yes	DR	DR
[19]	0.354	80.2	1.17 × 1.17 × 0.17	N/A	4.0%	Lateral	Yes	Feed	DR
[21]	2.465	20	0.45 × 0.23 × 0.18	4.5	5.3%	Broadside	Yes	DR + ground	DR
[22]	6.8	16	0.45 × 0.35 × 0.12	3.0	37.4%	Broadside	Yes	DR + feed + ground	DR
This work	2.5	$\begin{bmatrix} 13 & 0 & 0 \\ 0 & 21 & 0 \\ 0 & 0 & 13 \end{bmatrix}$	0.33 × 0.16 × 0.33	5.0	12.5%	Broadside	No	DR	DR

Table 1 gives an overview of several unidirectional LP DRAs in terms of size, gain, bandwidth, radiation and operating principle. Note that the proposed solution is the only one to solely use DR modes to obtain cardioid-shaped radiation pattern in the broadside direction.

6 | Conclusion

A uniaxial anisotropic DRA has been designed to obtain a Huygens source radiation pattern at 2.5 GHz. It is based on the combination of two co-located resonant modes within the DR that radiate as equivalent electric and magnetic dipoles. The uniaxial permittivity medium has given an additional degree of freedom to control the resonance frequencies of multiple modes in a DR.

3-D printing was used to manufacture the artificial anisotropic dielectric in a single process mixing zirconia and air, thus achieving these symmetric cardioid-shaped radiation patterns, without using ground planes or reflectors. The measurements agree reasonably with the simulations, resulting in a measured relative impedance bandwidth of 12.5% and a F/B ratio greater than 15 dB at the operating frequency.

These results demonstrate that achieving enhanced control of resonant modes by adjusting the effective permittivity tensor of artificial dielectrics through 3-D printing could unlock new possibilities in the advanced design of DRAs. This solution also opens up interesting prospects for the development of fully dielectric Huygens metasurfaces [60, 61].

Author Contributions

Carlos David Morales Peña: conceptualization, data curation, formal analysis, investigation, methodology, software, validation, visualization, writing – original draft. **Audric Boiteau:** conceptualization, data curation, formal analysis, investigation, methodology, software, validation, visualization, writing – original draft, writing – review and editing. **Christophe Morlaas:** conceptualization, data curation, formal analysis, funding acquisition, investigation, methodology, project administration, resources, software, supervision, validation, visualization, writing – original draft, writing – review and editing. **Alexandre Chabory:** conceptualization, data curation, formal analysis, funding acquisition, investigation, methodology, project administration, resources, software, supervision, validation, visualization, writing – original draft, writing – review and editing. **Romain Pascaud:** conceptualization, data curation, formal analysis, funding acquisition, investigation, methodology, project administration, resources, software, supervision, validation, visualization, writing – original draft, writing – review and editing. **Marjorie Grzeskowiak:** conceptualization, data curation, formal analysis, investigation, methodology, supervision, validation, visualization. **Gautier Mazingue:** conceptualization, data curation, formal analysis, investigation, methodology, supervision, validation, visualization.

Acknowledgements

The authors would like to thank the ENAC and the Région Occitanie for their financial support as well as C. Cailhol for his help in manufacturing and measuring the antenna. A. Boiteau also would like to thank the Agence de l'Innovation de Défense (AID) and the Centre National d'Études Spatiales (CNES) for the funding of his work.

Conflicts of Interest

The authors declare no conflicts of interest.

Data Availability Statement

The data that support the findings of this study are available from the corresponding author upon reasonable request.

References

1. S. R. Best, "The Significance of Ground-Plane Size and Antenna Location in Establishing the Performance of Ground-Plane-Dependent Antennas," *IEEE Antennas and Propagation Magazine* 51, no. 6 (December 2009): 29–43, https://doi.org/10.1109/map.2009.5433095.

2. L. Fernandez, M. Sobrino, J. A. R. de Azua, A. Calveras, and A. Camps, "Design of a Deployable Helix Antenna at L-Band for a 1-Unit Cubesat: From Theoretical Analysis to Flight Model Results," *Sensors* 22, no. 10 (2022): 3633, https://doi.org/10.3390/s22103633.

3. Y. Wang, M.-C. Tang, T. Shi, D. Yi, D. Li, and X. Zeng, "An Electrically Small Antenna With Quasi-Isotropic Coverage for Linearly Polarized Receiver," *IEEE Transactions on Antennas and Propagation* 70, no. 12 (December 2022): 11559–11568, https://doi.org/10.1109/tap.2022.3209755.

4. Y.-M. Pan, K. W. Leung, and K. Lu, "Compact Quasi-Isotropic Dielectric Resonator Antenna With Small Ground Plane," *IEEE Transactions on Antennas and Propagation* 62, no. 2 (February 2014): 577–585, https://doi.org/10.1109/tap.2013.2292082.

5. M.-C. Tang, Z. Wu, T. Shi, H. Zeng, W. Lin, and R. W. Ziolkowski, "Dual-Linearly Polarized, Electrically Small, Low-Profile, Broadside Radiating, Huygens Dipole Antenna," *IEEE Transactions on Antennas and Propagation* 66, no. 8 (August 2018): 3877–3885, https://doi.org/10.1109/tap.2018.2840835.

6. C. Ding, L. Zhang, J. Dong, and S. Gao, "Characteristic Mode Inspired Single-Plate Unidirectional Antenna Using Complementary Characteristic Radiation," *IEEE Transactions on Antennas and Propagation* 70, no. 10 (October 2022): 9837–9842, https://doi.org/10.1109/tap.2022.3177507.

7. Z. Wang and Y. Dong, "Theory, Design, and Verification of Miniaturized Phase-Controlled Huygens Antenna for 360° Continuous Beam Scanning," *IEEE Transactions on Antennas and Propagation* 71, no. 4 (April 2023): 3104–3113, https://doi.org/10.1109/tap.2023.3238646.

8. A. Chlavin, "A New Antenna Feed Having Equal E- and H-Plane Patterns," *IRE Transactions on Antennas and Propagation* 2, no. 3 (July 1954): 113–119, https://doi.org/10.1109/t-ap.1954.27983.

9. P. Alitalo, A. O. Karilainen, T. Niemi, C. R. Simovski, and S. A. Tretyakov, "Design and Realisation of an Electrically Small Huygens Source for Circular Polarisation," *IET Microwaves, Antennas & Propagation* 5, no. 7 (May 2011): 783–789, https://doi.org/10.1049/iet-map.2010.0524.

10. K.-M. Luk and H. Wong, "A New Wideband Unidirectional Antenna Element," *International Journal of Microwave and Optical Technology* 1 (June 2006): 35–44.

11. P. Jin and R. W. Ziolkowski, "Metamaterial-Inspired, Electrically Small Huygens Sources," *IEEE Antennas and Wireless Propagation Letters* 9 (2010): 501–505, https://doi.org/10.1109/lawp.2010.2051311.

12. M.-C. Tang, H. Wang, and R. W. Ziolkowski, "Design and Testing of Simple, Electrically Small, Low-Profile, Huygens Source Antennas With Broadside Radiation Performance," *IEEE Transactions on Antennas and Propagation* 64, no. 11 (November 2016): 4607–4617, https://doi.org/10.1109/tap.2016.2606552.

13. C. Morlaas, B. Souny, and A. Chabory, "Helical-Ring Antenna for Hemispherical Radiation in Circular Polarization," *IEEE Transactions on Antennas and Propagation* 63, no. 11 (November 2015): 4693–4701, https://doi.org/10.1109/tap.2015.2479640.

14. W. Lin and R. W. Ziolkowski, "Electrically Small, Low-Profile, Huygens Circularly Polarized Antenna," *IEEE Transactions on Antennas and Propagation* 66, no. 2 (February 2018): 636–643, https://doi.org/10.1109/tap.2017.2784432.

15. L. Guo, K. W. Leung, and Y. M. Pan, "Compact Unidirectional Ring Dielectric Resonator Antennas With Lateral Radiation," *IEEE Transactions on Antennas and Propagation* 63, no. 12 (December 2015): 5334–5342, https://doi.org/10.1109/tap.2015.2493579.

16. Y. M. Pan, K. W. Leung, and L. Guo, "Compact Laterally Radiating Dielectric Resonator Antenna With Small Ground Plane," *IEEE Transactions on Antennas and Propagation* 65, no. 8 (August 2017): 4305–4310, https://doi.org/10.1109/tap.2017.2712807.

17. L. Guo and K. W. Leung, "Compact Unilateral Circularly Polarized Dielectric Resonator Antenna," *IEEE Transactions on Antennas and Propagation* 66, no. 2 (February 2018): 668–674, https://doi.org/10.1109/tap.2017.2786346.

18. L. Guo, K. W. Leung, and N. Yang, "Wide-Beamwidth Unilateral Dielectric Resonator Antenna Using Higher-Order Mode," *IEEE Antennas and Wireless Propagation Letters* 18, no. 1 (January 2019): 93–97, https://doi.org/10.1109/lawp.2018.2881534.

19. R. E. Jacobsen, A. V. Lavrinenko, and S. Arslanagić, "A Water-Based Huygens Dielectric Resonator Antenna," *IEEE Open Journal of Antennas and Propagation* 1 (2020): 493–499, https://doi.org/10.1109/ojap.2020.3021802.

20. L. Guo and K. W. Leung, "Compact Linearly and Circularly Polarized Unidirectional Dielectric Resonator Antennas," *IEEE Transactions on Antennas and Propagation* 64, no. 6 (June 2016): 2067–2074, https://doi.org/10.1109/tap.2016.2536198.

21. M. Boyuan, J. Pan, S. Huang, D. Yang, and Y.-X. Guo, "Unidirectional Dielectric Resonator Antennas Employing Electric and Magnetic Dipole Moments," *IEEE Transactions on Antennas and Propagation* 69, no. 10 (October 2021): 6918–6923, https://doi.org/10.1109/tap.2021.3069556.

22. M. Boyuan, J. Pan, S. Huang, D. Yang, and Y.-X. Guo, "Wideband Endfire Dielectric Resonator Antenna Employing Fundamental and Higher Order Magnetoelectric Resonances," *IEEE Antennas and Wireless Propagation Letters* 20, no. 12 (December 2021): 2524–2528, https://doi.org/10.1109/lawp.2021.3117257.

23. C. D. Morales, C. Morlaas, A. Chabory, R. Pascaud, M. Grzeskowiak, and G. Mazingue, "Huygens Source Antenna Using Stacked Dielectric Resonators," in *2020 IEEE International Symposium on Antennas and Propagation and North American Radio Science Meeting*, (July 2020), 105–106.

24. S. Zhang, C. C. Njoku, W. G. Whittow, and J. C. Vardaxoglou, "Novel 3D Printed Synthetic Dielectric Substrates," *Microwave and Optical Technology Letters* 57, no. 10 (October 2015): 2344–2346, https://doi.org/10.1002/mop.29324.

25. L. Catarinucci, R. Colella, P. Coppola, and L. Tarricone, "Microwave Characterisation of Polylactic Acid for 3D-Printed Dielectrically Controlled Substrates," *IET Microwaves, Antennas & Propagation* 11, no. 14 (November 2017): 1970–1976, https://doi.org/10.1049/iet-map.2017.0498.

26. R. C. Rumpf, J. Pazos, C. R. Garcia, L. Ochoa, and R. Wicker, "3D Printed Lattices With Spatially Variant Self-Collimation," *Progress in Electromagnetics Research* 139 (2013): 1–14, https://doi.org/10.2528/pier13030507.

27. A. Goulas, S. Zhang, J. R. McGhee, et al., "Fused Filament Fabrication of Functionally Graded Polymer Composites With Variable Relative Permittivity for Microwave Devices," *Materials and Design* 193 (August 2020): 108871, https://doi.org/10.1016/j.matdes.2020.108871.

28. C. R. Garcia, J. Correa, D. Espalin, et al., "3D Printing of Anisotropic Metamaterials," *Progress In Electromagnetics Research Letters* 34 (July 2012): 75–82, https://doi.org/10.2528/pierl12070311.

29. S. P. Hehenberger, S. Caizzone, and A. Yarovoy, "Modeling and Measurement of Dielectric Anisotropy in Materials Manufactured Via Fused Filament Fabrication Processes," *Materials Research Bulletin* 179 (November 2024): 112938, https://doi.org/10.1016/j.materresbull.2024.112938.

30. Z. Wu, J. Kinast, M. E. Gehm, and H. Xin, "Rapid and Inexpensive Fabrication of Terahertz Electromagnetic Bandgap Structures," *Optics Express* 16, no. 21 (October 2008): 16442–16451, https://doi.org/10.1364/oe.16.016442.

31. Z.-X. Xia, K. W. Leung, and K. Lu, "3-D-Printed Wideband Multi-Ring Dielectric Resonator Antenna," *IEEE Antennas and Wireless Propagation Letters* 18, no. 10 (October 2019): 2110–2114, https://doi.org/10.1109/lawp.2019.2938009.

32. W. Albakosh, R. Asfour, Y. Khalil, and S. K. Khamas, "Wideband Millimeter-Wave Perforated Hemispherical Dielectric Resonator Antenna," *Electronics* 13, no. 9 (2024): 1694, https://doi.org/10.3390/electronics13091694.

33. R. S. Malfajani, H. Niknam, S. Bodkhe, D. Therriault, J.-J. Laurin, and M. S. Sharawi, "A 3D-Printed Encapsulated Dual Wide-Band Dielectric Resonator Antenna With Beam Switching Capability,"

IIEEE Open Journal of Antennas and Propagation 4 (2023): 492–505, https://doi.org/10.1109/ojap.2023.3274167.

34. Z.-X. Xia and K. W. Leung, "3-D-printed Wideband Circularly Polarized Dielectric Resonator Antenna With Two Printing Materials," *IEEE Transactions on Antennas and Propagation* 70, no. 7 (July 2022): 5971–5976, https://doi.org/10.1109/tap.2022.3161434.

35. A. Ávila Saavedra, M. Diaz, and F. Pizarro, "A 3D-Printed Enclosed Twist Dielectric Resonator Antenna With Circular Polarization," *Applied Sciences* 15, no. 2 (2025): 992, https://doi.org/10.3390/app15020992.

36. A. Buerkle, K. F. Brakora, and K. Sarabandi, "Fabrication of a DRA Array Using Ceramic Stereolithography," *IEEE Antennas and Wireless Propagation Letters* 5 (2006): 479–482, https://doi.org/10.1109/lawp.2006.885167.

37. A. A. Althuwayb, K. A. Abdalmalak, C. S. Lee, et al., "3-D-Printed Dielectric Resonator Antenna Arrays Based on Standing-Wave Feeding Approach," *IEEE Antennas and Wireless Propagation Letters* 18, no. 10 (October 2019): 2180–2183, https://doi.org/10.1109/lawp.2019.2939734.

38. C. Yang and K. W. Leung, "3-D-Printed Wideband Circularly Polarized MIMO Dielectric Resonator Antenna," *IEEE Transactions on Antennas and Propagation* 71, no. 7 (July 2023): 5675–5683, https://doi.org/10.1109/tap.2023.3270701.

39. S. Yarga, K. Sertel, and J. L. Volakis, "A Directive Resonator Antenna Using Degenerate Band Edge Crystals," *IEEE Transactions on Antennas and Propagation* 57, no. 3 (March 2009): 799–803, https://doi.org/10.1109/tap.2009.2013451.

40. S. Fakhte, H. Oraizi, and L. Matekovits, "High Gain Rectangular Dielectric Resonator Antenna Using Uniaxial Material at Fundamental Mode," *IEEE Transactions on Antennas and Propagation* 65, no. 1 (January 2016): 342–347, https://doi.org/10.1109/tap.2016.2627520.

41. S. Fakhte, H. Oraizi, L. Matekovits, and G. Dassano, "Cylindrical Anisotropic Dielectric Resonator Antenna With Improved Gain," *IEEE Transactions on Antennas and Propagation* 65, no. 3 (March 2017): 1404–1409, https://doi.org/10.1109/tap.2016.2647689.

42. S. Fakhte, I. Aryanian, and L. Matekovits, "Analysis and Experiment of Equilateral Triangular Uniaxial-Anisotropic Dielectric Resonator Antennas," *IEEE Access* 6 (2018): 63071–63079, https://doi.org/10.1109/access.2018.2877121.

43. F. Moayyed, H. R. D. Oskouei, and M. M. Shirkolaei, "High Gain and Wideband Multi-Stack Multilayer Anisotropic Dielectric Antenna," *Progress In Electromagnetics Research Letters* 99 (2021): 103–109.

44. M. Abedian, M. Khalily, F. Wang, P. Xiao, R. Tafazolli, and A. A. Kishk, "High Isolation Circularly Polarized In-Band Full-Duplex Anisotropic Dielectric Resonator Antenna," *Scientific Reports* 13, no. 1 (2023): 5937, https://doi.org/10.1038/s41598-023-31159-w.

45. Z.-K. Chen, L. Zhang, Z. Weng, and R.-Y. Li, "Wideband Wide-Beam Hybrid Dielectric Resonator Antenna Using Uniaxial Material," *IEEE Antennas and Wireless Propagation Letters* 22, no. 1 (January 2023): 124–128, https://doi.org/10.1109/lawp.2022.3204552.

46. C. D. Morales, C. Morlaas, A. Chabory, R. Pascaud, M. Grzeskowiak, and G. Mazingue, "3D-printed Ceramics With Engineered Anisotropy for Dielectric Resonator Antenna Applications," *Electronics Letters* 57, no. 18 (August 2021): 679–681, https://doi.org/10.1049/ell2.12234.

47. B. de Araùjo, C. Morlaas, R. Pascaud, A. Chabory, M. Grzeskowiak, and G. Mazingue, "3D-Printed Heterogeneous Isotropic–Anisotropic Dielectric Resonator for Singly Fed Dual-Band Circularly Polarised Antennas," *IET Microwaves, Antennas & Propagation* 18, no. 4 (April 2024): 220–230, https://doi.org/10.1049/mia2.12433.

48. S. Fakhte and L. Matekovits, "Controlling Frequency Distance Between Individual Modes of Dielectric Resonator Nanoantenna Using Uniaxial Anisotropic Materials," *Radiation Physics and Chemistry* 190 (2022): 109812, https://doi.org/10.1016/j.radphyschem.2021.109812.

49. A. D. Yaghjian, *Increasing the Supergain of Electrically Small Antennas Using Metamaterials* (3rd Eur. Conf. Antennas Propag., 2009), 858–860.

50. M. Zou and J. Pan, "Investigation of Resonant Modes in Wideband Hybrid Omnidirectional Rectangular Dielectric Resonator Antenna," *IEEE Transactions on Antennas and Propagation* 63, no. 7 (July 2015): 3272–3275, https://doi.org/10.1109/tap.2015.2425421.

51. Y.-Z. Liang, F.-C. Chen, W.-F. Zeng, and Q.-X. Chu, "Design of Self-Decoupling Dielectric Resonator Antenna With Shared Radiator," *IEEE Transactions on Antennas and Propagation* 71, no. 1 (2023): 1053–1058, https://doi.org/10.1109/tap.2022.3217118.

52. C. J. Ma, S. Y. Zheng, and Y. M. Pan, "Millimeter-Wave Co-Polarized In-Band Full-Duplex Antenna Based on a Mode Superposition Method," *IEEE Transactions on Antennas and Propagation* 71, no. 6 (June 2023): 4675–4685, https://doi.org/10.1109/tap.2023.3262339.

53. R. C. Rumpf, "Engineering the Dispersion and Anisotropy of Periodic Electromagnetic Structures," *Solid State Physics* 66 (2015): 213–300, https://doi.org/10.1016/bs.ssp.2015.02.002.

54. A. B. Numan and M. S. Sharawi, "Extraction of Material Parameters for Metamaterials Using a Full-Wave Simulator," *IEEE Antennas and Propagation Magazine* 55, no. 5 (October 2013): 202–211, https://doi.org/10.1109/map.2013.6735515.

55. G. Antoine, B. de Araujo, R. Pascaud, et al., "Comparison of Effective Permittivity Retrieval Methods of 3d-Printed Unit Cells for Dielectric Resonator Antenna Applications," in *Proc. 17th Eur. Conf. Antennas Propag. (EuCAP)*, (March 2023).

56. S. P. Hehenberger, S. Caizzone, S. Thurner, and A. G. Yarovoy, "Broadband Effective Permittivity Simulation and Measurement Techniques for 3-D-Printed Dielectric Crystals," *IEEE Transactions on Microwave Theory and Techniques* 71, no. 10 (October 2023): 4161–4172, https://doi.org/10.1109/tmtt.2023.3259479.

57. F. Doreau, C. Chaput, and T. Chartier, "Stereolithography for Manufacturing Ceramic Parts," *Advanced Engineering Materials* 2, no. 8 (August 2000): 493–496, https://doi.org/10.1002/1527-2648(200008)2:8<493::aid-adem493>3.0.co;2-c.

58. B. Li and K. W. Leung, "On the Differentially Fed Rectangular Dielectric Resonator Antenna," *IEEE Transactions on Antennas and Propagation* 56, no. 2 (February 2008): 353–359, https://doi.org/10.1109/tap.2007.915463.

59. A. Singh and S. K. Sharma, "Investigations on Wideband Cylindrical Dielectric Resonator Antenna With Directive Radiation Patterns and Low Cross Polarization," *IEEE Transactions on Antennas and Propagation* 58, no. 5 (May 2010): 1779–1783, https://doi.org/10.1109/tap.2010.2044330.

60. M. Decker, I. Staude, M. Falkner, et al., "High-Efficiency Dielectric Huygens' Surfaces," *Advanced Optical Materials* 3, no. 6 (June 2015): 813–820, https://doi.org/10.1002/adom.201400584.

61. S. M. Young and A. Grbic, "Dielectric Huygens' Metasurface Dome Antennas," *IEEE Antennas and Wireless Propagation Letters* 21, no. 11 (November 2022): 2181–2185, https://doi.org/10.1109/lawp.2022.3184595.